

Stoichiometry and surface reconstruction of epitaxial CuInSe₂(112) films

A. Hofmann and C. Pettenkofer

*Helmholtz-Zentrum Berlin, Institute for Silicon Photovoltaics, Albert-Einstein-Str. 15,
D-12489 Berlin, Germany*

CuInSe₂(112) films were grown on GaAs(111)A substrates by molecular beam epitaxy. The resulting surface stoichiometry was deduced by consideration of results from various surface analytic techniques. The obtainable Cu/In stoichiometry range in XPS was 0.4 – 1.2, where 1.2 marks the onset of Cu_{2-x}Se phase segregation at the surface and 0.4 corresponds to the copper-depleted surface with ordered defect compound (ODC) composition. For the stoichiometric CuInSe₂(112) surface, a c(4x2) reconstruction of the zinc blende surface periodicity is observed in the LEED pattern, with three rotational domains present on the flat GaAs(111) substrate. With the use of stepped (111) substrates, domain formation could be suppressed. By comparison of the LEED data and concentration depth profiles from angle-resolved XPS, two types of surface reconstructions could be distinguished. According to surface energy calculations in the literature, these correspond to surfaces stabilized by either Cu_{In} or 2V_{Cu} defects. The surface of copper-poor CuIn₃Se₅ shows no reconstruction of the zinc blende order.

1. Introduction

Thin-film solar cells based on chalcopyrite absorbers are the most efficient polycrystalline devices available today and also promising from the commercial point of view.¹ Although much effort has been made in the past years to optimize the efficiencies of devices, the knowledge about fundamental properties of chalcopyrite semiconductors is still limited. Therefore, our work is focused on the basic properties of the surfaces of CuInSe₂², the canonical chalcopyrite, to which most attention was paid in the past.

It is known for over 30 years that chalcopyrites can be grown epitaxially on Si and GaAs substrates^{3,4,5}. Bulk characterization techniques, like x-ray diffraction measurements confirmed the single-crystalline structure and chalcopyrite order of obtained films.⁶ Considering the surfaces, chalcopyrites exhibit fundamentally different properties compared to binary compound crystals with cubic lattice, for which the non-polar (110) face constitutes the most stable one. The growth of chalcopyrites on (110) zinc blende substrates by various techniques leads to a complete faceting into (112) surfaces of the tetragonal structure, which are the most stable surfaces for chalcopyrites^{7,8}. Well-ordered and reconstructed surfaces were observed for the (001) orientation for CuInSe₂⁹, CuGaSe₂¹⁰, CuInS₂¹¹. The natural growth surface in chalcopyrites is the (112), however, the signature of chalcopyrite order at the surface has not been observed yet.

Another peculiarity of chalcopyrites is the homogeneity range, which is much wider than for binary compounds. The ternary character implicates low defect formation energies, which can even become energetically favorable under certain conditions.¹² Depending on the growth conditions, Cu_{2-x}Se segregates on the surface or the Cu-poor CuIn₃Se₅ defect compound (β -phase) is present together with stoichiometric α -CuInSe₂. This phase segregation and defect formations leads to favorable electronic properties for Cu(In,Ga)Se₂ thin-film solar cells: grain boundaries are electrically benign,¹³ and it facilitates the type inversion at the absorber/buffer interface.¹⁴

To shed light on some of the unusual properties of chalcopyrite surfaces, we prepared CuInSe₂ films by molecular beam epitaxy (MBE) on GaAs(111)A substrates. Clean and well-ordered samples were thus obtained, which allow for detailed analysis of the CuInSe₂(112) surface. In order to avoid contamination, all preparation and analysis is performed in ultra-high vacuum (UHV). The influence of surface composition on the electronic properties is characterized by different surface analytical techniques. Surface unit cells for chalcopyrite surfaces are derived and contrasted with low-energy electron diffraction (LEED) data.

2. Experimental

CuInSe₂ samples were grown on flat GaAs(111)A substrates and on stepped GaAs(111)A with 5° miscut towards [100] direction. The GaAs wafer pieces were wet chemically prepared, which consisted of an etching step followed by surface passivation with (NH₄)₂S¹⁵, prior to insertion into the UHV system. For MBE deposition, the substrates were heated to 525°C, while the Se shutter was opened to provide a Se ambient prior to growth. Residues of the sulfur passivation are removed during this procedure. The Cu and In sources were opened simultaneously, and the cation ratio was adjusted by varying the Cu effusion cell temperature. The cation to anion ratio is self-adjusting if Se provided in excess and the growth rate was roughly 5 nm/min.

Most of the surface analysis was performed in our integrated UHV system, with a base pressure in the low 10⁻¹⁰ mbar range. Here, different deposition and analysis methods are accessible without contaminating the sample surface. X-ray and ultra-violet photoelectron spectroscopy (XPS/UPS) was carried out using x-ray sources which generate MgK_α or monochromatized AlK_α radiation, a He gas discharge lamp and a Specs Phoibos 150 electron analyzer. An Omicron SpectraLEED was used for LEED measurements.

The angle-resolved XPS measurements for concentration depth profiling were partly carried out at the Solias endstation, which was connected to the U49/2-PGM-2 beamline at BESSY II. During the transfer to the synchrotron, the sample surface was covered with a protective Se layer which can be removed without altering the surface properties by annealing the sample to 250°C¹⁶.

3. Results

a. Sample characterization and surface stoichiometry

Due to their ternary character, chalcopyrites exhibit a wide range of possible stoichiometries, especially with respect to the Cu/In ratio. CuInSe₂ mixes with the binary phases Cu_{2-x}Se and In₂Se₃¹⁷, and also with its Cu-poor defect phases, of which the most prominent are CuIn₃Se₅ and CuIn₅Se₈¹⁸. For a correct interpretation of our results, the knowledge about the surface stoichiometry is therefore mandatory. However, in order to derive elemental concentration ratios from XP spectra, the intensity of photoemission

peaks needs to be normalized with sensitivity factors, which depend on photoionization cross section (PICS), electron mean free path and electron analyzer characteristics¹⁹. Additionally, the participating elements can have depth-dependent concentration gradients as a result of surface reconstruction, which can not be resolved by a simple XPS measurement.

Due to the issues mentioned above, different routes were followed for a reliable determination of the crucial Cu/In surface concentration ratio from the Cu2p_{3/2} and In3d_{5/2} photoemission lines. For the following considerations, the sensitivity factors published by Moulder *et al.* were used, where a Cu2p_{3/2}/In3d_{5/2} peak area ratio of 0.79 corresponds to a concentration ratio 1¹⁹. Due to differences in the experimental systems, the error of surface stoichiometry ratios is expected to be still large (25%), but the relative changes for different samples shown here should exhibit a much better accuracy.

The validity of the obtained concentration ratios is further endorsed by an analysis of the Cu Auger parameter α_{Cu}. Here, the binding energy of the Cu 2p_{3/2} peak and the kinetic energy of the Cu L₃M₄₅M₄₅ Auger emission are added, whereby shifts from surface band bending and doping are cancelled out. This results in a very sensitive measure for the chemical environment of Cu atoms near the surface. For Cu-rich surface compositions (Cu/In > 1), α_{Cu} increases from 1849.5 eV towards values of 1850.0 eV and more, which is indicative of the Cu_{2-x}Se phase (see FIG 1). On the In-rich side, a lock-in of α_{Cu} at values around 1849.40 – 1849.45 eV is observed, which is only slightly reduced to roughly 1849.35 eV for strong Cu depletion. This coincides with the literature value for CuInSe₂²⁰ and apparently also holds for the strongly Cu-poor defect compounds. The lock-in at Cu/In ≈ 1 further proves the correctness of our analysis.

Next we will consider the position of the valence band maximum (VBM) in UP spectra, which gives information about the position of the Fermi level inside the band gap and hence on the surface doping. The binding energy of the VBM is determined by linear extrapolation of the leading edge of the valence band to the background intensity. The stoichiometry-dependent VBM are plotted in FIG 1. For Cu-rich compositions, small or zero VBM are observed in general, which means p-type conduction at the surface or segregation of a metallic phase, respectively. In case of near-stoichiometric or slightly Cu-poor compositions, the Fermi-level resides near mid-gap,

with rather strong variations between samples of comparable stoichiometry. On the strongly Cu-depleted side, the VBM reaches values up to 1.2 or 1.3 eV and therefore exceeds the CuInSe₂ bulk band gap determined from photoluminescence of 1.05 eV⁶. This finding is usually explained with a band gap opening of the Cu-poor surface, and the associated n-type conductivity is characteristic of In-rich films with ordered defect compound composition²¹. The large values for VBM could also partially be attributed to surface band bending. A shift of the spectra after illumination with a halogen lamp was, however, not observed.

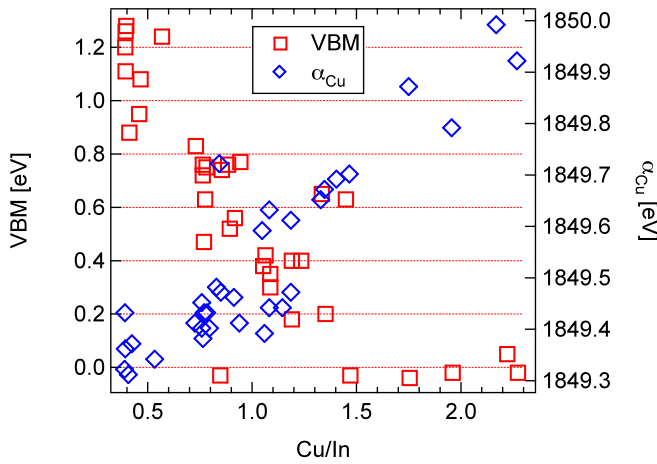


FIG 1 Binding energy of the valence band maximum with respect to the Fermi level for CuInSe₂(112) films with varying Cu/In surface concentration ratio. The position of the VBM was determined by linear extrapolation of the leading edge in HeI UP spectra. Also displayed are the Cu Auger parameters α_{Cu} for different Cu/In ratios.

All results considered together give a convincing and conclusive conception about the stoichiometry determined for the CuInSe₂ surfaces. However, the stated stoichiometry ratios do not claim to be exact, due to the discussed reasons. Yet the variety of data shows satisfactory agreement and a comprehensive picture.

b. CuInSe₂ LEED pattern

When growing chalcopyrites on binary semiconductors, the reduced symmetry of the chalcopyrite lattice compared to the zinc blende lattice needs to be considered. It was pointed out earlier by Tiwari *et al.* that CuInSe₂ grows in three domains rotated by 120° on cubic (111) substrates²². Additionally, twinning is expected for chalcopyrite. We will elucidate the implications of domain formation on GaAs(111) substrates later and start with

the deduction of the unit cell of the chalcopyrite (112) surface from the truncated bulk structure.

If the CuInSe₂ crystal is truncated in a (112) plane above a cation layer, a rectangular surface unit cell results that is defined by the chalcopyrite order of Cu and In atoms. The unit cell comprises 4 cations and is enlarged compared to the hexagonal unit cell of the zinc blende lattice. The zinc blende order is still present in the anion layers formed solely by Se atoms. By calculating the reciprocal lattice vectors, the surface unit cell can be translated into the surface Brillouin zone (SBZ) for CuInSe₂, which is also rectangular. This SBZ constitutes a c(4x2) reconstruction compared to the zinc blende surface order. Symmetry points of the surface BZ were constructed and labeled according to the procedure in²³ and symmetry points of the bulk chalcopyrite BZ were taken from²⁴ (see FIG 2).

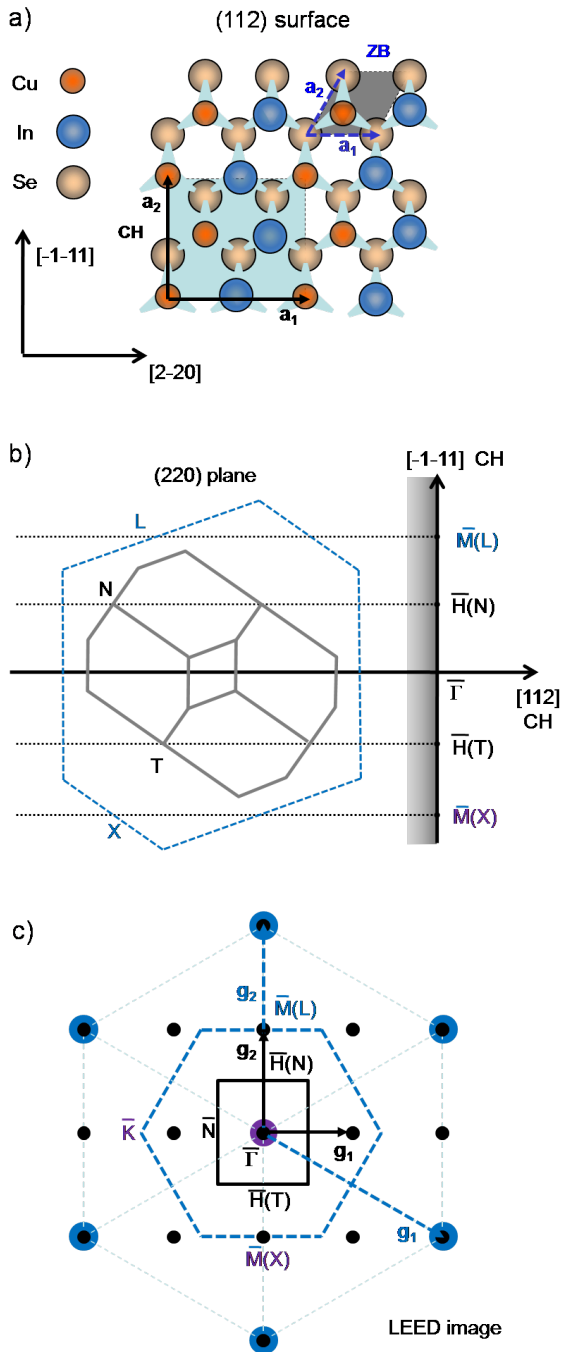


FIG 2 a) Cation-terminated $\text{CuInSe}_2(112)$ surface atom arrangement as given by the bulk chalcopyrite structure. Surface unit cell vectors for zinc blende (dashed blue lines) and chalcopyrite (solid black lines) are indicated. b) Construction to derive symmetry points of the chalcopyrite surface Brillouin zone from the bulk BZ. c) SBZ of the zinc blende and the chalcopyrite (111)/(112) surface and corresponding LEED patterns.

This surface superstructure which is derived from the bulk chalcopyrite order, shall now be compared with experimental data. In order to obtain $\text{CuInSe}_2(112)$ with a single rotational domain, the samples were grown on stepped $\text{GaAs}(111)\text{A}$ wafers. Due to the miscut, the wafer exhibits terraces that suppress domain formation by step-flow growth along the step edges. The resulting LEED images of the near-stoichiometric $\text{CuInSe}_2(112)$ ($\text{Cu}/\text{In} = 1.1$) surface in FIG 3 show clearly a $c(4 \times 2)$ single-domain

reconstruction of the zinc blende surface. Stretching of the LEED spots indicates the direction perpendicular to the surface steps, which is the $[-1-11]$. Therefore, the $[1-10]/[-110]$ direction is aligned with terrace edges.

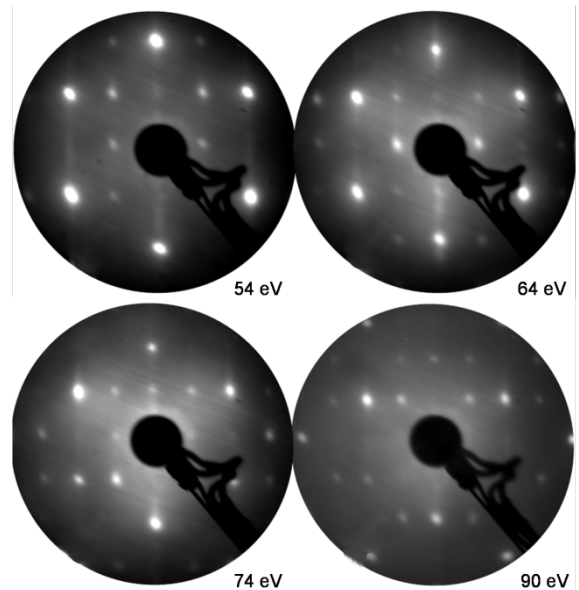


FIG 3 LEED images for the $\text{CuInSe}_2(112)$ surface. The sample was grown on a stepped $\text{GaAs}(111)\text{A}$ substrate in order to obtain one rotational domain. A surface Cu/In ratio of 1.10 was determined with XPS.

First-principles calculations of the cation-terminated $\text{CuInSe}_2(112)$ surface suggests different reconstructions models, depending on the cation chemical potential^{25,26}. For the stoichiometric and In-rich surface, a reconstruction involving 2 copper vacancies (V_{Cu}) per surface unit cell is the most stable configuration. On the Cu-rich side, a reconstruction with one Cu-on-In antisite defect (Cu_{In}) per surface unit cell is energetically favorable. Both reconstructions leave (the size of) the surface unit cell unaffected, which corresponds to the observed $c(4 \times 2)$ superstructure of the zinc blende pattern. Hence, this chalcopyrite surface unit cell is energetically favorable over a large composition range.

c. Effect of stoichiometry variation

In order to further elucidate the effect of stoichiometry variations on the surface order and LEED pattern, $\text{CuInSe}_2(112)$ surfaces with different stoichiometries were prepared on $\text{GaAs}(111)\text{A}$ wafers, this time without miscut and hence a flat surface. The lower symmetry of the chalcopyrite compared to the zinc blende lattice leads to the formation of domains when growing CuInSe_2 on a GaAs substrate. These domains, which are rotated by 120° around the (112) axis have

been observed by different experimental techniques²². The expected resulting LEED pattern is shown in FIG 4.

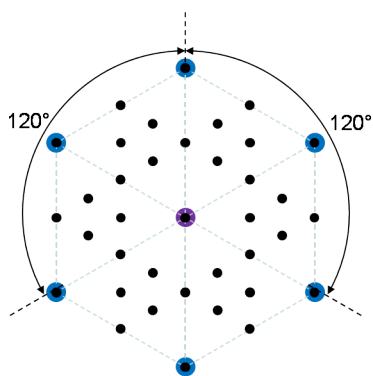


FIG 4 Resulting LEED image for the zinc blende (111) surface with 3 rotational domains of c(4x2) reconstruction.

In order to classify the obtainable LEED images for the CuInSe₂(112), three composition ranges, each with a characteristic pattern shall be defined:

1. A slightly Cu-rich surface composition, which corresponds to the Cu_{in} antisite surface structure.
2. The near-stoichiometric and slightly In-rich surface, which is expected to be stabilized by the 2 V_{Cu} defects.
3. The strongly Cu-depleted surface with the stoichiometry of the ordered defect compound CuIn₃Se₅.

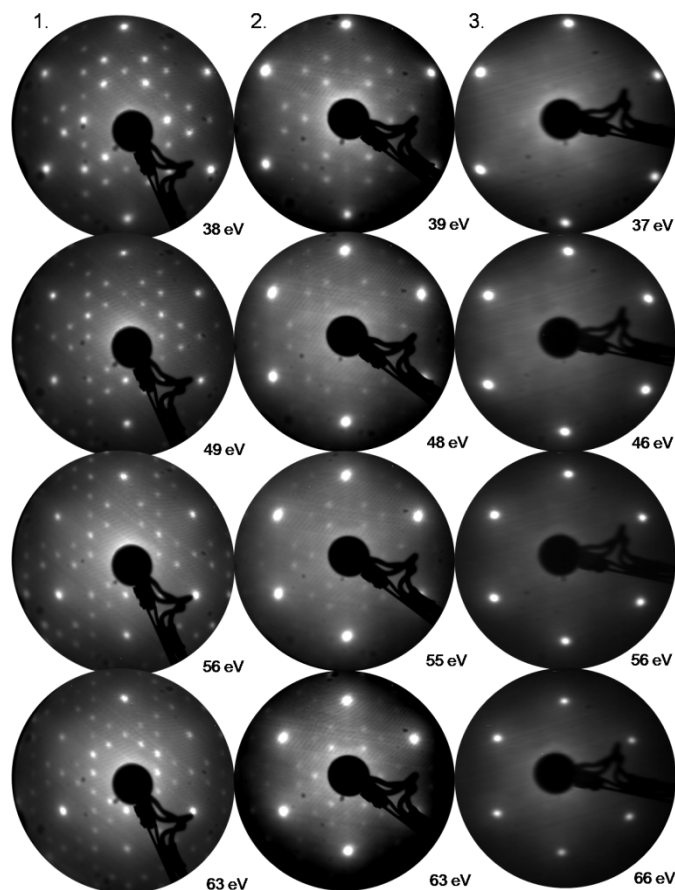


FIG 5 The three types of LEED images of CuInSe₂(112) surface (rotational domains) which correspond to the three composition regimes 1. Cu-rich, Cu/In = 1.19. 2. Near-stoichiometric / In-rich, Cu/In = 0.79. 3. Defect compound, Cu/In = 0.39.

LEED images for different kinetic energies for each type of surface composition are shown in FIG 5. The following characteristics can be distinguished:

1. This type of LEED image could only be obtained by using copper rich growth conditions and subsequent annealing in selenium atmosphere. The surface stoichiometry from XPS with MgK α radiation yields Cu/In ratios around 1.2. The spots of the c(4x2) reconstruction pattern with rotational domains appear all sharp, bright and clearly visible throughout the displayed energy range. Compared to the following surface stoichiometry cases, the intensity difference of the zinc blende spots compared to the chalcopyrite superstructure spots is low. This poses another experimental verification of the theoretically predicted c(4x2) reconstruction.
2. A small reduction of copper flux during the experiment yields the type of LEED pattern displayed below. Here, the surface Cu/In ratio is typically around 1. We observe intense yet broadened zinc blende main spots and comparably weak superstructure spots. The diffuse background is again low, proofing the order of the surface.

Apart from the reduced intensity of the superstructure spots, there is another peculiarity compared to the Cu-rich case: The superstructure spots on the tie-line between main spots are suppressed for most of the electron kinetic energy range and appear only weakly for certain kinetic energies. This kind of intensity modulation is usually understood as a result of the three-dimensional atomic structure, which means the influence of atomic layers below the surface layer. Yet the observed pattern and therefore the atomic arrangement in the surface plane still corresponds to a $c(4 \times 2)$ reconstruction.

3. For strongly copper-poor preparation conditions, Cu/In ratios around 0.4 are obtained near the surface. Here, superstructure spots are entirely missing and only the hexagonal pattern of the unreconstructed zinc blende surface is visible for any of the displayed energies. The spots are again slightly broadened and intense with low background. This shows that for strong copper depletion, the chalcopyrite order at the surface is lifted.

Hence, different types of surface compositions can be distinguished from the characteristics of their LEED patterns. How do the different surface compositions affect the valence band structure?

d. UPS Valence band structure

Each of the presented types of LEED patterns also owns a characteristic shape of the valence band density of states measured by UPS. Using UV HeI photons, the spectra presented in FIG 6 are obtained in normal emission. Since we investigated epitaxial samples, the shape of the photoemission spectra is not only influenced by the density of states and PICS of the valence band states, but also reflects the three-dimensional band structure in k -space. Therefore, the spectra are also affected by the excitation energy and emission angle².

For the Cu-rich surface, the valence band appears very structured with many clearly distinguishable emission maxima which correspond to individual or close-lying groups of electronic bands. In particular, three states appear near the VBM. A strong maximum resides at $E_B = 3.0$ eV which corresponds to the non-bonding Cu3d bands, the valence band gap and bonding Cu-Se bands below $E_B = 4$ eV as well as another minimum and the In-Se states around $E_B = 7$ eV can be separated.

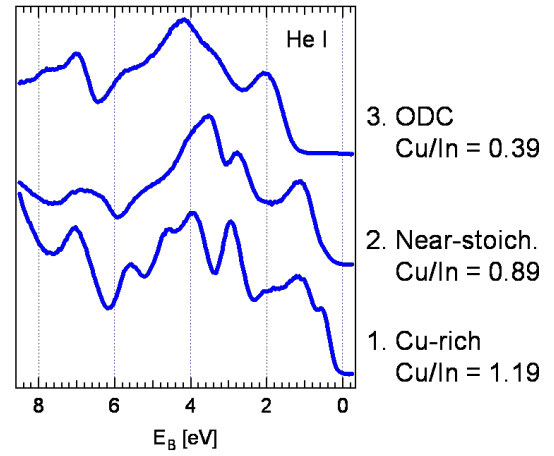


FIG 6 Photoemission spectra ($h\nu = 21.2$ eV) of the $\text{CuInSe}_2(112)$ valence band (normal emission) for the three stoichiometry regimes.

The transition to the In-rich near stoichiometric sample shows less maxima and structure, the Cu3d emission at $E_B = 2.8$ eV is reduced compared to the remainder of VB features. A DOS gap represented by a minimum at $E_B = 3.2$ eV can, however, still be observed (see also²). The rearrangement of electronic states continues for further copper reduction. The valence band defect structure does not show a minimum related to the DOS gap at $E_B = 3.6 - 3.8$ eV. Instead, the middle part of the valence band is formed by a broad block of states that is weakly structured. This makes the identification of individual states impossible and can be explained with an increased number of bands in the Cu-poor material

18 27

e. Concentration depth profile

To track possible stoichiometry variations in the near-surface region, concentration depth profiles for different compositions were measured by angle-resolved XPS. This method makes use of the fact that the escape depth of photoelectrons and therefore the information depth of XPS, can be reduced by tilting the detected emission angle ϑ away from the surface normal. If ϑ is the detected emission angle and λ is the inelastic mean free path (IMFP) of electrons in the solid, then the escape depth is $\lambda_{\text{eff}} = \lambda \cos\vartheta$. This λ_{eff} is also a measure for the information depth, since 95% of primary electrons in XPS are emitted within $3 \lambda_{\text{eff}}$ from the surface²⁸. By tilting the sample, concentration depth profiles can be obtained for flat and ordered surfaces like those of the epitaxial CuInSe_2 films.

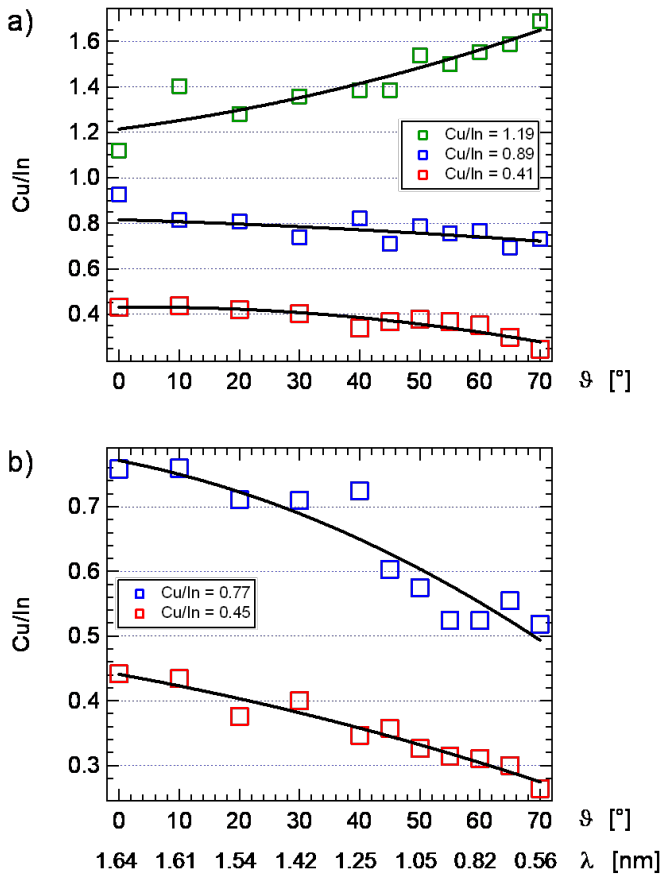


FIG 7 a) Cu/In ratios from AR-XPS using AlK $_{\alpha}$ radiation for samples with different surface stoichiometries. Note that the information depths for the copper and indium signal are different. b) AR-XPS data using synchrotron radiation with $h\nu = 1133$ eV for Cu2p emission and $h\nu = 645$ eV for In3d emission. The resulting mean free paths for electrons with $E_{kin}=200$ eV in CuInSe $_2$ are also stated²⁹.

One series of Cu/In ratio depth profiles for samples with different surface stoichiometries was recorded using mono-AlK $_{\alpha}$ ($h\nu = 1486.6$ eV) radiation for the excitation of photoelectrons. The Cu/In ratios were calculated from the intensities of Cu2p $_{3/2}$ and In3d $_{5/2}$ core level emissions, corrected by the sensitivity factors provided in section 3.1. The use of a common excitation energy for Cu2p $_{3/2}$ and In3d $_{5/2}$ electrons implies different kinetic energies and hence different information depths for both elemental species, which is a drawback of this method. According to work by Seah and Dench²⁹, λ for Cu2p $_{3/2}$ electrons in CuInSe $_2$ corresponds to 2.6 nm, while In3d $_{5/2}$ electrons own a larger λ of 3.6 nm.

The sample stoichiometries stated in FIG 7 were determined from XPS measurements with MgK $_{\alpha}$ radiation, like it was done throughout this article. By increasing the detected emission angle, the surface sensitivity of the measurement increases. For the Cu-rich sample, this leads to an increase in Cu/In ratio. On the other hand, for slightly In-rich/near-stoichiometric sample, the Cu/In decreases slightly with reduced

information depth. The decrease is even more pronounced for the strongly Cu-depleted surface.

Another data set was recorded using synchrotron radiation (FIG 7b) in order to adjust the excitation energy in such a way that electrons from the Cu2p $_{3/2}$ and In3d $_{5/2}$ core levels are emitted at the same kinetic energy of 200 eV. This corresponds to a λ of 1.6 nm²⁹. The PE intensities were normalized by PICS from³⁰ and the photon flux measured with a GaAs diode. Here, an indium-rich surface shows a strong reduction of Cu/In for decreasing λ_{eff} . The same behavior is observed for the surface with defect compound stoichiometry.

For the synchrotron radiation measurement, λ_{eff} changes from 1.6 to 0.56 nm for the displayed range of emission angles. Within this range of information depths, a strong change in composition is observed. We can therefore conclude that the observed depletion or enrichment of copper is restricted to the first few atomic layers near the surface. An analog experiment on epitaxial CuInSe $_2$ (112) samples by Liao *et al.*²⁸ using MgK $_{\alpha}$ radiation resulted in very similar behavior for the In-rich surface. By simulation of the concentration depth profile, they obtained a copper-depletion of the first 1-2 atomic layers. The observed changes in Cu/In ratios can therefore be associated with surface reconstructions. The reconstructions exhibit excess Cu for Cu-rich surface compositions and a Cu depletion in case of In-rich and stoichiometric surface compositions.

4. Discussion

Thus we arrive at a very complete picture about the stoichiometry and reconstruction of cation-terminated CuInSe $_2$ (112) surfaces. According to first-principles calculations, the copper-rich surface is stabilized by Cu $_{In}$ defects which conserve the chalcopyrite unit cell²⁶. Sharp spots in the LEED pattern with a clear superstructure and distinct features in the valence band proof the superior quality of material grown under copper-rich conditions³¹. The simultaneous presence of Cu-rich protrusions was recently proven in a photoelectron microscopy study of the epitaxial films³².

For the near-stoichiometric and indium-rich surface, the concentration depth profile coincides with the results from Liao *et al.*²⁸, which indicates a 2V $_{Cu}$ reconstruction. The LEED patterns proof that, although

with a reduced long-range order, the chalcopyrite order is still present at the surface. Due to the coexistence of copper-poor β -phases in the bulk, the defect density is enhanced compared to the Cu-rich material. The presence of these two reconstructions, each associated with a $c(4 \times 2)$ surface ordering is consistent with the result of surface energy calculations²⁶.

A Cu-poor surface reconstruction is also observed for the defect compound material CuIn_3Se_5 . Apparently, the Cu concentration near the surface is again reduced compared to the bulk, probably forming a copper-free reconstruction. However, no calculations are available for the defect compound surface.

In the literature, the Cu-depleted defect compound surface of chalcopyrite absorbers in solar cells was explained in terms of the Cu-free reconstruction of the predominant (112) surface. This was found by Liao *et al.*²⁸ for epitaxial samples and by Mönig *et al.*³³ for the polycrystalline material with slightly Cu-poor integral composition. According to first-principles calculations, this surface stills exhibits chalcopyrite order, like it was observed for the slightly indium-rich case. We explain the absence of chalcopyrite order at the surface by the sphalerite order of the bulk defect compound. In case of strong Cu-depletion, the chalcopyrite order is lifted for the bulk and consequently also at the surface. The ordering of defects predicted by theory is apparently short-range.

All the results stated above were obtained for chalcopyrite grown on GaAs(111)A substrates, for which a cation-terminated surface is expected. The $c(4 \times 2)$ reconstruction could also be observed for

samples grown on GaAs(111)B and Si(111) substrates. We therefore conclude that the $c(4 \times 2)$ reconstruction exist for both, cation and anion terminated near-stoichiometric $\text{CuInSe}_2(112)$ surfaces, in agreement with calculation²⁶.

Experimental data on the (112) surface ordering of chalcopyrites are scarce. An early LEED study found a hexagonal zinc blende pattern for $\text{CuInSe}_2(112)$ without superstructure³⁴. For $\text{CuInSe}_2(112)$ on stepped Si(111), a faint (2×1) reconstruction was observed³⁵. In contrast to our findings, these surface orderings cannot be related to chalcopyrite structure.

On the other hand, clear LEED images were obtained for the polar $\text{CuInSe}_2(001)$ surface⁹. The investigated films were grown by MBE on GaAs(001) substrates¹⁶ and showed a mixed $(4 \times 2)/(2 \times 4)$ reconstruction with facets. This could be converted into a single-domain (4×2) structure by combined Ar^+ sputtering and annealing treatment. The (4×2) reconstruction is consistent with our results for $\text{CuInSe}_2(001)$ ² and corresponds to an enlargement of the surface unit cell compared to the chalcopyrite order. This leaves the possibility that a true chalcopyrite surface is present here, however, (4×2) reconstructions can also occur on zinc blende (100) surfaces³⁶.

In summary, we have demonstrated the stoichiometry dependence of the $\text{CuInSe}_2(112)$ surface reconstruction. Three composition regimes could be identified, each with a characteristic LEED pattern, valence band structure and concentration depth profile. The results could be related to defect-stabilized surface reconstructions predicted by first principles calculations.

¹ M. A. Green, K. Emery, Y. Hishikawa, W. Warta, Prog. Photovoltaics **18**, 346 (2010).

² A. Hofmann, C. Pettenkofer, Phys. Rev. B **84**(11), 115109 (2011).

³ B. Schumann, C. Georgi, A. Tempel and G. Kühn, Thin Solid Films **52**, 45 (1978).

⁴ A. N. Tiwari, S. Blunier, K. Kessler, V. Zelezny and H. Zogg, Appl. Phys. Lett. **65**, 2299 (1994).

⁵ S. Niki, Y. Makita, A. Yamada, O. Hellman, P.J. Fons, A. Obara, Y. Okada, R. Shioda, H. Oyanagi, T. Kurafuji, S. Chichibu and H. Nakanishi, J. Cryst. Growth **150**, 1201 (1995).

⁶ S. Niki, P. J. Fons, A. Yamada, T. Kurafuji, S. Chichibu, H. Nakanishi, W. G. Bi and C. W. Tu, Appl. Phys. Lett. **69**, 647 (1996).

⁷ B. Schumann, A. Temple and G. Kühn, Solar Cells **16**, 43 (1986).

⁸ D. Liao and A. Rockett, J. Appl. Phys. **91**, 1978 (2002).

⁹ T. Deniozou, N. Esser, T. Schulmeyer, R. Hunger., Appl. Phys. Lett. **88**(5), 052102 (2006).

¹⁰ T. Deniozou, N. Esser, S. Siebentritt, P. Vogt, R. Hunger. Thin Solid Films, **480-481**, 382 (2005). EMRS 2004.

¹¹ W. Calvet, Präparation und in-situ Charakterisierung MBE-gewachsener Kupferindiumdisulfid-Schichten. PhD thesis, BTU Cottbus (2002).

¹² S.B. Zhang, S.-H. Wei and A. Zunger, Phys. Rev. Lett. **78**, 4059 (1997).

¹³ S. Siebentritt, S. Sadewasser, M. Wimmer, C. Leendertz, T. Eisenbarth and M.-C. Lux-Steiner, Phys. Rev. Lett. **97**, 146601 (2006).

-
- ¹⁴ A. Niemegeers, M. Burgelman, R. Herberholz, U. Rau, D. Hariskos and H.-W. Schock, *Prog. Photovolt. Res. Appl.* **6**, 407 (1998).
- ¹⁵ K. Ueno, T. Shimada, K. Saiki, A. Koma, *Appl. Phys. Lett.* **56**(4), 327 (1990).
- ¹⁶ R. Hunger, T. Schulmeyer, A. Klein, W. Jaegermann, K. Sakurai, A. Yamada, P. Fons, K. Matsubara, S. Niki. *Surface Science*, **557**(1-3), 263 (2004).
- ¹⁷ J.S. Park, Z. Dong, S. Kim, J.H. Perepezko, *J. Appl. Phys.* **87**, 3683 (2000).
- ¹⁸ S. B. Zhang, S.-H. Wei, A. Zunger. *Phys. Rev. B* **57**, 9642 (1998).
- ¹⁹ J. F. Moulder, W. S. Stickle, P. E. Sobol, und K. D. Bomben. *Handbook of X-ray Photoelectron Spectroscopy*. Physical Electronics Inc., Minnesota, USA (1995).
- ²⁰ E. Niemi, L. Stolt. *Surface and Interface Analysis* **15**(7), 422 (1990).
- ²¹ M. Bär, S. Nishiwaki, L. Weinhardt, S. Pookpanratana, O. Fuchs, M. Blum, W. Yang, J. D. Denlinger, W. N. Shafarman, C. Heske. *Appl. Phys. Lett.* **93**, 244103 (2008).
- ²² M. Krejci, A. N. Tiwari, H. Zogg, P. Schwander, H. Heinrich, und G. Kostorz. *Journal of Applied Physics*, **81**(9), 6100 (1997).
- ²³ R. Courths, H. Wern, S. Hüfner. *Solid State Comm.* **61**(4), 257 (1987).
- ²⁴ J. L. Shay und J. H. Wernick. *Ternary chalcopyrite semiconductors: growth, electronic properties, and applications*. Pergamon Press (1975).
- ²⁵ J. E. Jaffe, A. Zunger. *Phys. Rev. B* **64**(24), 241304 (2001).
- ²⁶ S. B. Zhang, S.-H. Wei. *Phys. Rev. B* **65**(8), 081402 (2002).
- ²⁷ A. Hofmann, *Elektronische Struktur epitaktischer Chalkopyrite und deren Heterokontakte für die Photovoltaik*. PhD thesis, BTU Cottbus (2011).
- ²⁸ D. Liao, A. Rockett. *Appl. Phys. Lett.* **82**(17), 2829 (2003).
- ²⁹ M. P. Seah, W. A. Dench. *Surface and Interface Analysis*, **1**(1), 2 (1979).
- ³⁰ J. J. Yeh, I. Lindau. *Atomic Data and Nuclear Data Tables*, **32**(1), 1 (1985).
- ³¹ A. M. Gabor, J. R. Tuttle, D. S. Albin, M. A. Contreras, R. Noufi, A. M. Hermann. *Appl. Phys. Lett.* **65**, 198 (1994).
- ³² C. Pettenkofer, A. Hofmann, W. Bremsteller, C. Lehmann, F. Kelleter. *Ultramicroscopy* accepted.
- ³³ H. Mönig, C.-H. Fischer, R. Caballero, C. Kaufmann, N. Allsop, M. Gorgoi, R. Klenk, H.-W. Schock, S. Lehmann, M. Lux-Steiner, I. Lauer mann. *Acta Materialia*, **57**(12), 3645 (2009).
- ³⁴ P. Corvini, A. Kahn, S. Wagner. *J. Appl. Phys.* **57**, 2967 (1985).
- ³⁵ R. Hunger, C. Pettenkofer, R. Scheer. *Surface Science* **477**, 76 (2001).
- ³⁶ C.H. Park, D.J. Chadi, *Phys. Rev. B* **49**, 16467 (1994).